Arabian Journal of Chemistry (2023) **16**, 104411

King Saud University

Arabian Journal of Chemistry

www.ksu.edu.sa
www.sciencedirect.com

ORIGINAL ARTICLE

Rosmarinus officinalis extract as eco-friendly corrosion inhibitor for copper in 1 M nitric acid solution: Experimental and theoretical studies

Badreah A. Al Jahdaly

Chemistry Department, Faculty of Applied Science, Umm Al-Qura University, Makkah, Saudi Arabia

Received 11 September 2022; accepted 7 November 2022
Available online 12 November 2022

KEYWORDS

Rosmarinus officinalis;
Electrochemical;
Corrosion;
Copper

Abstract Rosmarinus officinalis extract (ROE) was studied chemically (mass loss, ML), electrochemically impedance spectrometry (EIS), and potentiodynamic polarization (PDP) as a corrosion inhibitor in 1 M nitric acid. According to ML, ROE is effective like a copper preservative in 1 M HNO_3 acid solution at R.T by improving inhibitor concentration up to 77 % at 300 ppm and 25 °C. A study was conducted regarding the effect of temperature on copper adsorption, as well as the calculation of adsorption coefficients. Results indicated that physisorption increases with temperature, indicating a decrease in inhibition efficiency (%IE). Langmuir's adsorption model was consistent with the adsorption mechanism. Using the PDP method, the inhibitor accumulated on the copper surface in mixed forms. Moreover, EIS revealed that the value of double-layer capacitance dropped with an increased dose of ROE, while the charge transfer resistance improved. A different approach was taken to the examination of surfaces. Both theoretical studies and practical results were calculated and compared to demonstrate that the results were valid.

1. Introduction

Ancient civilizations used copper to create bronze mirrors, coinage, and copper seals (Hoffman, 2019). However, it is now directly tied to copper, whether it be the ongoing functioning of cars, the unavoidable comfortable ventilation, or the soaring missiles (Hussain, 2020; Marques et al., 2020; Scott and Schwab, 2019). Copper has always had strong links to social life and industrial endeavors because of its outstanding electrical and thermal conductivity. The pickling procedure is frequently used to guarantee the metal's quality (Galai et al., 2017). The corrosion of copper in acidic conditions is unsatisfactory (Zhang et al., 2020). Corrosion inhibitors are frequently employed in corrosion protection because of their low cost and excellent effectiveness (Palanisamy, 2019). Therefore, corrosion inhibitors can be added to pickling solutions to overcome this problem. Corrosion inhibitor application offers multiple benefits, including small volume, simple operation, low cost, wonderful effect, great compatibility, and more (Al Jahdaly et al., 2021; Agboola et al., 2022). Plant extracts are among the most popular green corrosion inhibitors because of how simple they are to prepare, the variety of materials they may be manufactured of, and how little harm they cause to people and the environment. In general, it is simple to access fresh plant tissues, and the extraction pro-

E-mail address: bajahdali@uqu.edu.sa
Peer review under responsibility of King Saud University.

Production and hosting by Elsevier

https://doi.org/10.1016/j.arabjc.2022.104411
1878-5352 © 2022 The Author(s). Published by Elsevier B.V. on behalf of King Saud University.

cedure is rapid, simple, and eco-friendly, all of which are helpful to further improve overall preparations (Zhang et al., 2022; Huang et al., 2022; Kumari et al., 2022). Because amino acids, polyphenols, and flavonoids provide a protective barrier on the metal's surface, these substances are found in the extracts as many functional groups, including (N—O—P—S) (Loto et al., 2022; Loto, 2020; Odunlami et al., 2021). There is a good number of antioxidants in ROE like such as methyl carnosate, rosmarinic acid, carnosic acid, rosmadial, rosmanol, and epirosmanol with phenolic diterpenoide. A phytochemical analysis of R. officinalis extracts has revealed that it contains rosmarinic acid, camphor, caffeic acid, ursolic acid, betulinic acid, carnosic acid, and carnosol (El Faydy et al., 2016). Consequently, R. Officinalis contains mostly phenolic compounds, diterpenes, and essential oils (Kadiri et al., 2018). R. officinalis L. leaves are commonly used as an analgesic, antibacterial, and carminative in traditional medicine (Miraj and Kiani, 2016; Kompelly et al., 2019). Besides treating minor wounds, rashes, headaches, dyspepsia, and circulatory issues, rosemary oil and extracts may also be used for expectorants, diuretics, and antispasmodics. It appears that Rosmarinus officinalis extract acts as an anticorrosion metal when used in acidic environments, as it protects XC48 steel from corrosion.The chemical composition of these compounds is outlined in Table 2. In this study, an eco-friendly, nontoxic substance namely a Rosmarinus officinalis extract (ROE) will be evaluated for its potency against the copper dissolution in an acidic medium (1.0 M nitric acid solution) by using chemical, electrochemical methods, Fourier transform infrared (FTIR), scanning electron microscopy (SEM) as well as characterization techniques from Monte Carlo simulation and density functional theory DFT to discover the adsorption type and corrosion mechanism on the metal surface.

2. Experimental methods

2.1. Materials and solutions

Pieces of copper of certain chemical compositions were used as listed in Table 1. 2x2 cm^2 (height breadth) was the coupon's dimensions. Prior to beginning, the Cu surface was scraped with silicon carbide emery sheets varying in grade from 100 to 1500, and it was carefully scrubbed with D.W. Furthermore, samples were cleaned with acetone (Hamadi et al., 2018). Nitric acid was purchased from Sigma-Aldrich Chemicals Company with a concentration of 70 percent, and it was diluted to reach the desired concentration.

2.2. Mass loss

For the measurements of mass loss, copper samples with a thickness of 2.0 * 2.0 * 0.2 cm were used, which were polished to different degrees of sandpaper, then washed with alcohol to remove impurities and dirt, distilled water, and then the process of good drying of the samples, followed by mass loss measurements by the usual methods at different temperatures which calculated according to the following equation (Xiao et al., 2022; Kadhim et al., 2021):

$$\%IE = \theta x100 = 1 - \frac{W}{W_O} x100 \quad (1)$$

W and W^O are the mass loss of metal without and with investigated compounds, respectively.

2.3. Electrochemical measurements:

Electrochemical measurements were performed at a temperature of 25 °C with platinum electrodes, calomel electrodes, and copper electrodes. As part of this system, platinum electrodes were used as counters, calomel electrodes as references, and copper electrodes as working electrodes (Fergachi et al., 2019). A copper electrode dipped in an acidic medium at an open circuit voltage obtained a semi-stable state. An alternating current signal of 5 mv was used to determine inhibition efficiency by measuring impedance at various times and varying frequencies among 10^{-2} and 10^{-5} Hz and the IE% was calculated by using the following equation (Singh et al., 2019):

$$IE\% = \frac{R_{ct} - R_{ct,0}}{R_{ct}} \times 100 \quad (2)$$

R_{ct} and $R_{ct,0}$ are charge-transfer resistances of inhibited and uninhibited copper, respectively.

An experiment was performed to determine the polarization value at 1 mV s-1 and in the −250 mV range. The following equation was used to calculate inhibitory efficiency values (Chen et al., 2020).

$$IE\% = \frac{i_{corr,0} - i_{corr}}{i_{corr,0}} \times 100 \quad (3)$$

$i_{corr,0}$, and i_{corr} mean current density values lack the existence of the protection of compounds. With a computer monitor attached to Potentiostat/Galvanostat/ZRA. A Gamry framework system based on the ESA 400 is included. EIS300 and DC105 polarization software are also included in Gamry applications.

2.4. Surface characterization:

The copper surface was screened in detail in both its inhibitor- and inhibitor-free states using the Scanning Electron Microscope (SEM - Quattro S) technique. Two copper pieces were submerged in nitric acid alone (Blank) and another in nitric acid with 300 ppm of ROE combinations for 48 h in this experiment (Onyeachu et al., 2022; Saleh et al., 2022).

2.5. Theoretical calculation

Through Materials Studio's Dmol3 module, the quantum chemical properties of ROE are computed. Geometry optimization is the mathematical operation, GGA and PBE are the functional operators, DNP is levied as the basis set and a COMPASS was the force field (Chkirate et al., 2021; Shahmoradi et al., 2021; Pal and Das, 2022).

Table 1 Lists the mass percentages of the copper metal's chemical composition.

Element	As	Pb	Bi	Fe	Sn	Ag	Cu
mass percentages	0.0002	0.002	0.0005	0.01	0.001	0.001	The rest

Table 2 ROE's primary ingredients' chemical composition.

A (Carnosic acid)	**B** (Rosmarinic acid)	**C** (Carnosol)
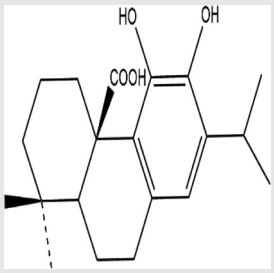	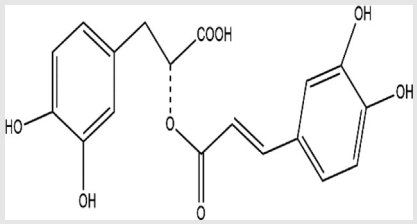	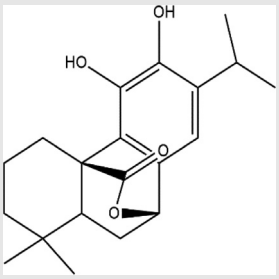

3. Results and Discussion

3.1. Extract characterization

Rosmarinus officinalis extract IR spectra were obtained using SPEACTUM-65 (PerkinElmer® FT-IR spectrometer) in the region of 4000 – 400 cm^{-1}. Fig. 1 shows the different infrared spectra of the various groups present in the extract. The presence of vibration at 3371 cm^{-1} is related to the presence of a hydroxyl group (O—H) bond (Boukaoud et al., 2021). At 1684 cm^{-1}, a sharp peak is attributed to the carbon–oxygen or carbonyl group (C═O), and another vibration at 1016 cm^{-1} is associated with the presence of a (C—O) single bond (Mintz et al., 2021). We note the occurrence of vibration between 1016 and 1455 cm^{-1} associated with the presence of a Carboxylic acid's (O—H) bond (Karolina et al., 2022; Jiang et al., 2021). The most important compounds found in ROE are rosmarinic acid, carnosic acid, and carnasol, which are primarily responsible for the presence of antioxidants, inflammation, and anti-carcinogenic (Esmeeta et al., 2022; Erigoni, 2021).

3.2. Mass loss method

Based on Table 3 and Fig. 2, we show the results of Cu mass loss in 1.00 M HCl in the absence or presence of amended inhibitor doses. According to Table 3, Cu corrosion rates in 1.0 M HCl were inhibited by all tested doses of the inhibitor. Inhibitor dose affects corrosion rate. It is evident that IE rises as inhibiting concentration increases (Alaoui et al., 2016).

3.3. Adsorption isotherm

The isotherm of adsorption is useful in determining the inhibition pathway. Also, isotherm diagrams can be used to visualize the inhibitor-metal interaction. It was tested if Langmuir, Freundlich, and Temkin diagrams were best suited for the task (Alaoui et al., 2016). Fig. 3 illustrates the approximate right correlation coefficient. A Langmuir adsorption isotherm can be observed in 1.0 M nitric acid solutions where ROE molecules adsorb with correlation coefficients and slopes close to 1. The K_{ads} The intersections of the lines could be used to cal-

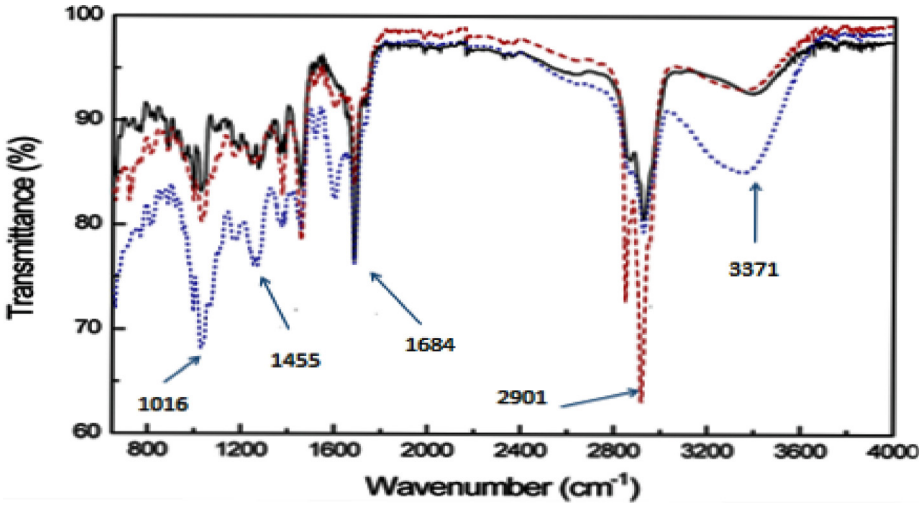

Fig. 1 IR spectrum of the different Rosmarinus officinalis extracts.

Table 3 Different measurements of inhibition for the corrosive effects of 1 M HNO_3 on copper with different doses both with and without ROE at 25 °C.

[inh], ppm	θ	%IE
50	0.271	27.1
100	0.448	44.8
150	0.626	62.6
200	0.672	67.2
250	0.72	72.0
300	0.77	77.0

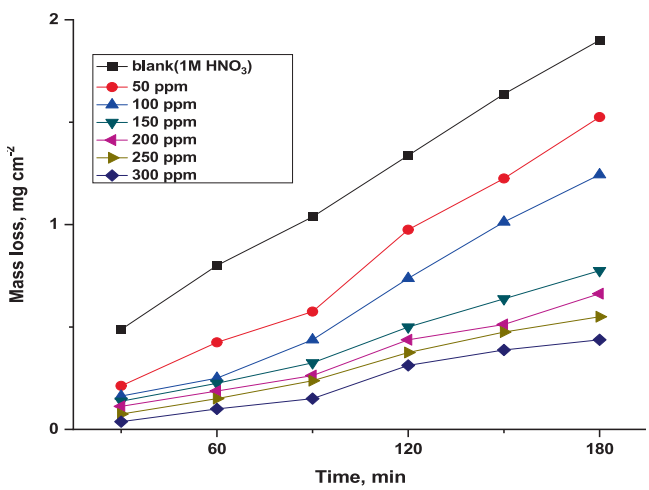

Fig. 2 Effect of immersion times on mass loss of Cu in 1 M HNO_3 with and without different doses of ROE at 25 °C.

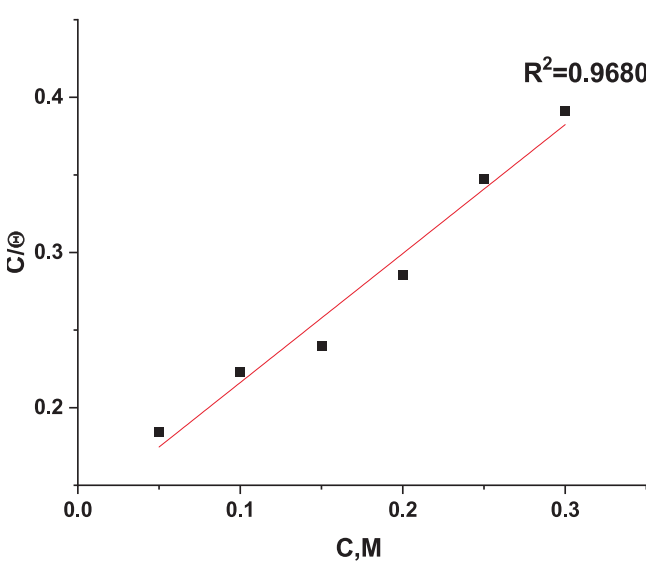

Fig. 3 Langmuir adsorption plot as C/θ vs C, M of ROE for corrosion of copper in 1 M HNO_3 solution at 25 °C.

culate values. on the C/θ-axis and K_{ads} was connected to the standard adsorption-free energy ΔG^o_{ads} as follows:

$$\frac{C}{\theta} = \frac{1}{K_{ads}} + C \tag{4}$$

The value of the adsorption constant K_{ads} was calculated, and through it, the free energy ΔG^o_{ads} values were computed using the equation:

$$K = \frac{1}{55.5} exp^{\frac{-\Delta G_{ads}}{RT}} \tag{5}$$

Table 4 illustrates that the ROE molecules are thought to be electrostatically interconnected in an acidic solution when the $\Delta G°_{ads}$ value is around − 20 kJ mol^{-1} or lower, while a value of − 40 kJ mol^{-1} or higher indicates a charge exchange or transfer between the copper surface and the ROE molecules (Jafari et al., 2022). Using $\Delta G°_{ads}$, it was confirmed that physical adsorption had taken place. The $\Delta G°_{ads}$ enthalpy values resulting from electrostatic interactions between charged molecules and charged metal (physisorption) range up to 41.9 kJ mol^{-1}, whereas those, resulting from chemisorption, range up to about 100 kJ mol^{-1}. Physisorption produces molecules with small absolute enthalpy values. When the examined chemicals are present, $\Delta S°_{ads}$ values were negative and large, indicating the increase in the ordering on the copper surface (Zhang et al., 2019).

3.4. Potentiodynamic polarization (PDP) measurements

As shown in Fig. 4, copper polarization in a 1 M HNO3 medium is characterized by typical curves. It is evident from the polarization curve that both current and voltage have increased in value until they have reached their highest peak without inhibition (Yang et al., 2019; Abd El Aziz et al., 2022). In response to the formation of Cu (NO3)2, the current value rapidly decreased after reaching its maximum value. The inhibitor significantly reduced cathodic and anodic current density. A change in the E_{corr} value is also noticed in the presence of (ROE). If the E_{corr} displacement is greater than 85 mV, an inhibitor may be classified as cathodic or anodic; otherwise, it may be classified as mixed. The current study indicates that the examined inhibitor is a mixed-type inhibitor because the maximum displacement in Ecorr is 85 mV (Yan et al., 2020). In Fig. 4, higher (ROE) concentrations inhibit Cu electrode anodic corrosion. Also, the cathodic reaction is suppressed to a lesser extent when (ROE) is present. As shown in Table 5, there is a reduction in anodic dissolution by ROE and a delay in hydrogen evolution reaction due to ROE, which results in values of βa that are higher than those obtained by a blank in the absence of ROE. Hence, the oxidation mechanism is suppressed by the (ROE), which controls the anodic reactions on the metal surface (Benarioua et al., 2019).

3.5. Electrochemical impedance spectroscopy (EIS) measurements

We have also applied the EIS approach to investigate the corrosion behavior of copper in 1 M nitric acid solution, both in the lack and existence of various ROE concentrations (Dhouibi et al., 2021). Nyquist plots presented imperfect semicircles with a time constant due to the rough surface of the copper electrode. The diameter of the capacitive ring increases significantly when the inhibitor is added to the 1 M solutions of HNO_3, and this improvement becomes more pronounced as the doses of the inhibitor raise. These observations indicate the adsorption of inhibitory molecules on the copper surface

Table 4 ROE adsorption data on a copper surface at various temperatures in 1 M HNO_3.

Temperature,°C	$K_{ads} \times 10^{-3}$ M^{-1}	$-\Delta G°_{ads}$ kJ/mol	$\Delta H°_{ads}$ kJ/mol	$\Delta S°_{ads}$ J mol^{-1}
25	8.8683	15.36	67.59	278.38
30	20.533	17.73		281.62
35	37.11952	19.54		282.92
40	45.599	20.39		281.13
45	51.177	21.0		278.69

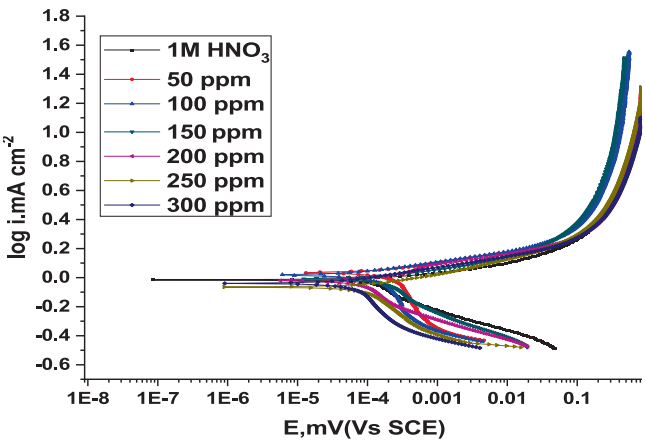

Fig. 4 Potentiodynamic polarization curves for the dissolution of copper in 1 M HNO_3 in the lack and existence of various doses of ROE at 25 °C.

and the creation of a protective film. This film reduces the active surface area of copper, improves its corrosion resistance, and greatly inhibits copper corrosion in the 1 M HNO_3 solution (Zhang et al., 2021). The impedance data in Table 6 indicate that the R_{ct} value increases as the inhibitor dose increases (Fouda et al., 2021), and this indicates that the inhibitory effect becomes stronger in acidic solutions and this was proved by calculating the chi-square (χ2) values shown in Table 7. Due to this, a protective layer is formed at the metal solution contact during copper dissolution, and a single semicircle was observed, suggesting that a single charge transfer mechanism took place and that this mechanism was unaffected by the bound molecule (Bedair et al., 2021). When the inhibitor dose increases, the capacitance of the double layer diminishes. There is a density difference between the electrical double layer and the insulating layer. A polarization and mass loss approach yield similar results in terms of percent IE acquisition.

All capacitance elements in Fig. 5 are replaced with constant phase elements (CPEs), namely CPE_f and CPE_{dl}. A solution resistance is represented by Rs, and a passive film's capacitance is represented by CPE_f. In passive films, R_f corresponds to the ionic resistance. Double layer corrosion area's capacitive behavior is described by CPE_{dl}, while charge transfer resistance is expressed as Rct (Zuñiga-Diaz et al., 2020). As shown in (Fig. 6a and Fig. 6b), Nyquist and Bode plots for Cu corrosion in 1 M HNO3 solution are plotted based on phase angle and frequency (Charoen-amornkitt et al., 2020). Calculate the double-layer capacitance, C_{dl}, for a circuit from the following equation:

$$C_{dl} = Y_O(\omega_{max})n - 1 \quad (6)$$

whereY_0 is the magnitude of the CPE, $\omega_{max} = 2\pi f_{max}$, f_{max} is the frequency at which the imaginary component of the impedance is maximal and the factor n a lies between 0.50 and 1.0 (Laschuk et al., 2021). The similarity of the general shape of the curves (in the presence or absence of an inhibitor) shows that there is no change in the corrosion mechanism. As a further evidence, Bode plots inhibited by a phase angle increase were shown to have a greater degree of phase angle. The morphology of protected surfaces improved with an increase in phase angle values (Zhang et al., 2019). A concentration of ROE results in an enlargement in Nyquist curve diameters and phase angle values in Bode plots (Fig. 6b).

3.6. SEM examination

SEM experiments verify the adsorption of a layer of ROE on the copper surface. Fig. 7(a-c) show SEM micrographs of the surface of Cu alone and after 48 h of immersion in 1 M HNO_3 with adding 300 ppm of ROE. The metal surface appears clearly, while in the absence of ROE, we find clear damage to the copper surface due to the corrosion of HNO_3 (Fig. 7b). Nevertheless, the metal surface does not appear to corrode when compared to the examined compound (Fig. 7c). It was found that a thin layer of the extract formed on the surface of the copper, thus protecting the surface from corrosion.

3.7. Quantum chemical analysis

The stabilized molecular configuration of carnosic acid, rosmarinic acid, and carnosol is shown in Fig. 8, together with

Table 5 Corrosion potential (e_{corr}), corrosion current density (i_{corr}), Tafel slopes (β_a, β_c), degree of surface coverage(θ), and inhibition efficiency (%IE) of copper in 1 M HNO_3 at 25 °C for ROE.

Inhibitor	[inh] ppm	$-E_{corr}$ Mv vs SCE	I_{corr}x10^{-4} μA cm-2	βa, mV dec^{-1}	βc, mV dec^{-1}	C.R mpy	Θ	%IE
Blank	0	16.20	512.0	318.7	−222.3	252.6	0.0	0.0
ROE	50	45.00	66.40	72.30	−207.3	32.75	0.870	87.0
	100	39.30	65.80	70.60	−188.8	32.47	0.871	87.1
	150	42.50	64.70	74.50	−198.4	31.92	0.874	87.4
	200	49.10	37.60	58.50	−203.1	18.56	0.926	92.6
	250	89.30	33.50	99.80	−227.9	16.53	0.935	93.5
	300	83.10	28.00	70.90	−216.7	13.83	0.945	94.5

Table 6 Copper electrochemistry kinetics in HNO3 with and without ROE concentrations.

Inhibitor	[inh] ppm	R_{ct}, $\Omega\ cm^2$	R_s x10^{-3}, $\Omega\ cm^2$	C_{dl} x10^{-4}, μFcm^{-2}	Θ	% IE
Blank	0	28.60	968.1	6.045	0.0	0.0
ROE	50	39.35	982.6	2.8	0.273	27.3
	100	63.98	910.5	5.83	0.553	55.3
	150	84.22	1778	4.45	0.660	66.0
	200	112.5	1463	3.83	0.746	74.6
	250	134.2	844.1	9.72	0.787	78.7
	300	231.3	827.4	2.41	0.876	87.6

Table 7 Chi Square (χ2) of $R_{ct.}$

Observed Value 1	Expected Value1	Chi Square 1 X 10^{-4}	Observed Value 2	Expected Value 2	Chi Square 2 X 10^{-6}	Observed Value 3	Expected Value 3	Chi Square 3 X 10^{-4}
28.512	28.612	4.400	28.661	28.656	111	28.908	28.729	10.203
39.352	39.285	1.071	39.352	39.349	0.0151	39.386	39.445	1.090
63.964	63.891	0.731	63.983	63.995	3.918	64.154	64.152	0.430
84.211	84.073	2.233	84.223	84.210	1.125	84.273	84.416	2.542
112.110	112.286	3.092	112.521	112.469	8.430	112.933	112.740	2.149
133.703	133.944	4.483	134.221	134.163	0.101	134.751	134.491	3.223
231.271	230.926	3.231	231.324	231.303	0.0487	231.643	231.861	3.144

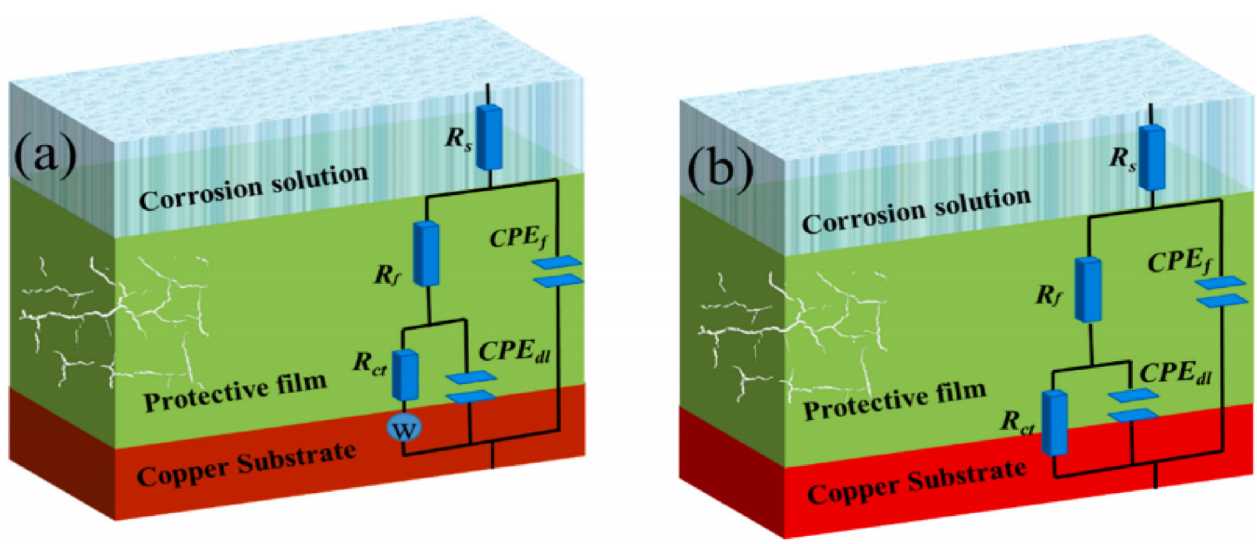

Fig. 5 Equivalent circuit model used to fit experimental EIS.

the associated border molecular orbital distribution graphs. The HOMO and LUMO orbitals represent the molecular structure's capacity to give and accept electrons, respectively (Choudhary et al., 2019). There are oxygen atoms, —OH, and C═O groups, and hydroxyl groups in all components of the extract, which act as electron donors (HOMO), and benzene rings that act as acceptors (LUMO). The energy gap (ΔE) can be calculated based on these two energies. The energy gap (ΔE) and dipole moment (μ) values of Carnosic acid, Rosmarinic acid, and Carnosol. As shown in 10(a), the ΔE values of Carnosic acid, Rosmarinic acid, and Carnosol are 4.620 eV, 3.093 eV, and 5.284 eV, respectively. Previous researchers have revealed a relationship between decreased energy gaps and higher inhibitor efficiencies (Chen et al., 2020; Errahmany et al., 2020). A molecular orbital surface with a low unoccupied molecular orbital surface (LUMO) appears along with

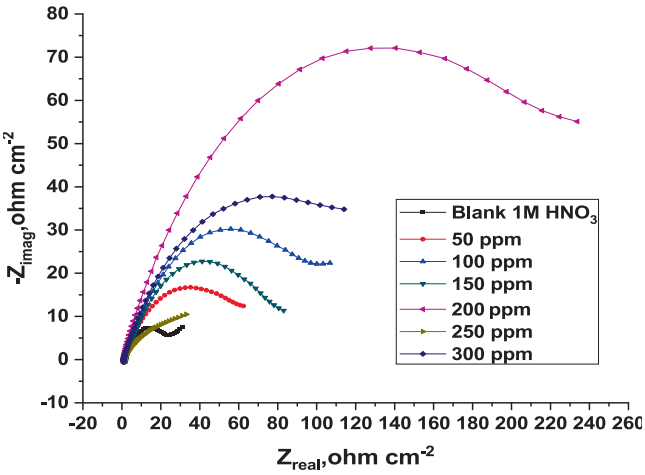

Fig. 6a Copper corrosion plots in 1 M HNO_3 without and with ROE at 25 °C.

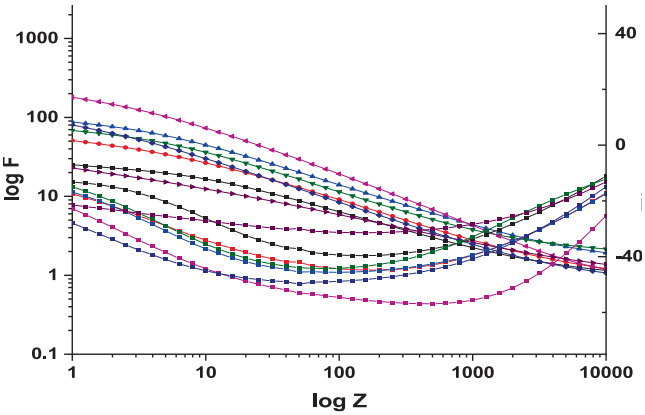

Fig. 6b The Bode plots for the corrosion of copper in 1 M HNO_3 in the lack and existence of various concentrations of ROE at 25 °C.

its highest occupied molecular orbital surface (HOMO). Surfaces with HOMO or LUMO charge indicate which sites of the molecule might donate electrons to the metal, and surfaces with LUMO charge indicate which electrons would be regifted to the inhibitor (Sayed and El-Lateef, 2020; Hadisaputra et al., 2020). A HOMO is primarily defined by oxygen atoms and the π bond on the benzene ring that is responsible for resonance. At the same time, the LUMO is centered around carbon atoms. The ΔE value has the potential to estimate the inhibitor molecule's reactivity to the metal atom; lower ΔE values may indicate better inhibition efficiency (Obi-Egbedi et al., 2011; Niamien et al., 2012). From these DFT calculations and the trends described, it was defined that Rosmarinic acid (ΔE = 3.082) as shown in Table 8 behaved as a superior corrosion inhibitor relative due to its lower ΔE. On the other hand, the dipole moment (DM) does not play an essential role in determining the efficiency of inhibition (Rodríguez-Valdez et al., 2005).

3.8. Molecular dynamics analysis

The adsorption structure of carnosic acid, rosmarinic acid, and carnosol at the Cu(1 1 1) surface is depicted in Fig. 9 in the gaseous state. At the Cu(1 1 1) interface, carnosic acid, rosmarinic acid, and carnosol are mostly adsorbed in addition to adsorption to achieve a high level of protection for the Cu substrate (Belakhdar et al., 2020). Following adsorption to the Cu (1 1 1) interface, their binding energy is determined by formulas (6) and (7):

$$E_{interact} = E_{tot} - (E_{sub} + E_{inh}) \quad (6)$$

$$E_{Binding} = -E_{interact} \quad (7)$$

A list of the binding energies of carnosic acid, rosmarinic acid, and carnosol is presented in Table 9. The $E_{Binding}$ of Rosmarinic acid on the Cu (1 1 1) interface is signally greater than that of Carnosic acid and Carnosol. Therefore, Rosmarinic acid plays a vital effect in the adsorption of ROE onto the copper interface. It is evident from E_{ads} negative results that the copper substrate was strongly adsorption with carnosic acid, rosmarinic acid, and carnosol (Galai et al., 2020). Compared to Carnosic acid, and Carnosol, Rosmarinic acid exhibits greater adsorption energy, indicating it performs better as an inhibitor for copper protection in 1.0 M nitric acid. All available data is accurate and supported by this theoretical analysis. Lastly, (ROE) inhibitors offer great protection against corrosion.

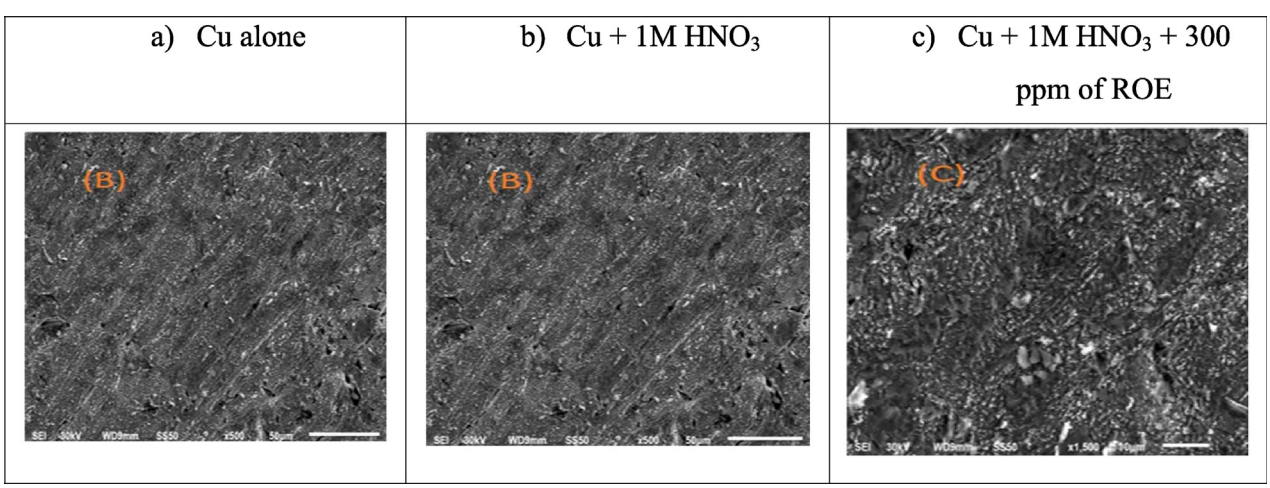

Fig. 7 SEM micrographs of the surface of Cu alone and after immersion in 1 MHNO_3

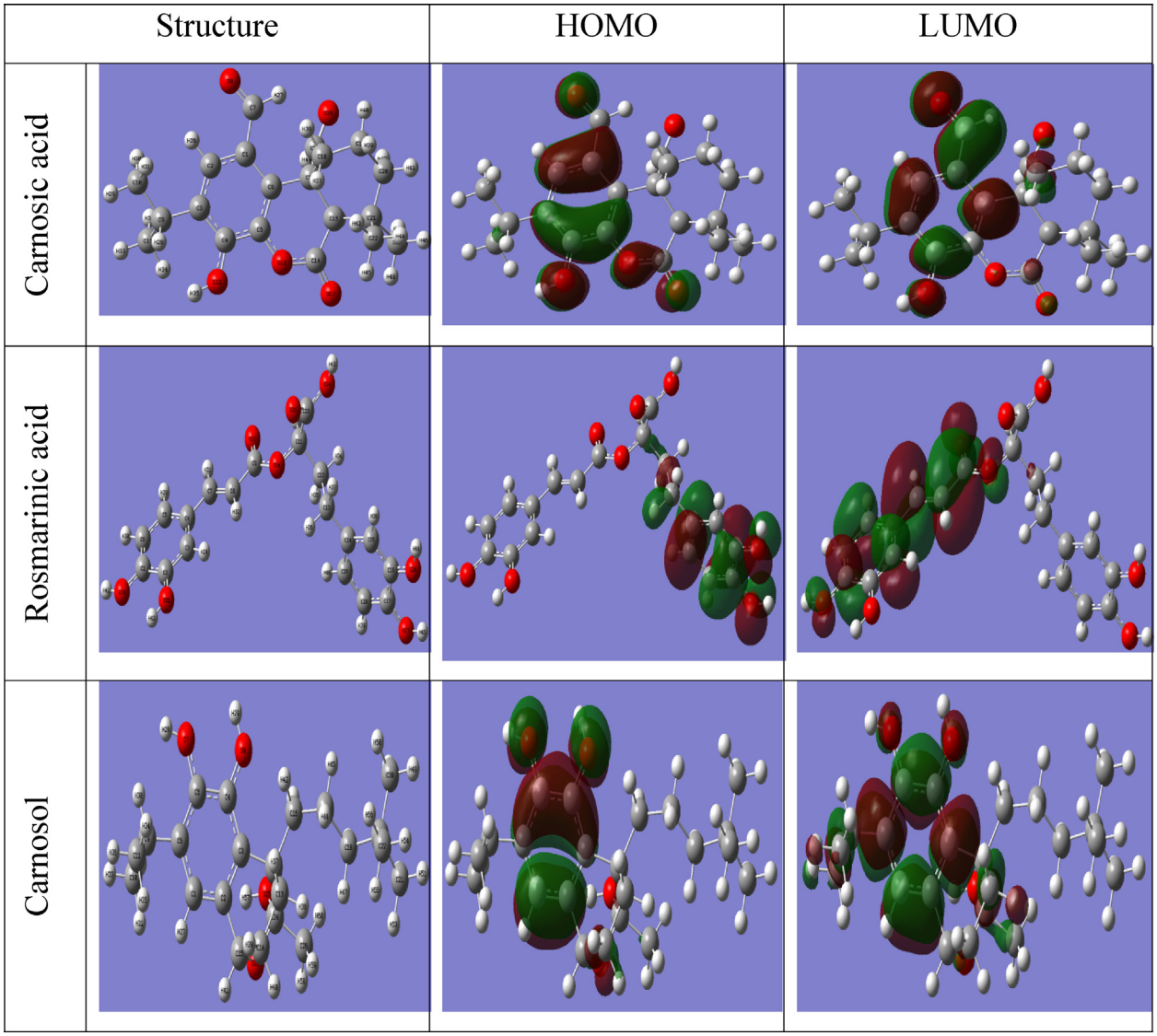

Fig. 8 Optimized structure, HOMO, and LUMO of ROE components.

Table 8 Quantum Chemical parameters.

Structure	E_{HOMO}	E_{LUMO}	$\Delta E = E_{LUMO}$-E_{HOMO}	Dipole moment
Carnosic acid	−6.386	−1.766	4.620	3.2100
Rosmarinic acid	−5.299	−1.526	3.093	2.4760
Carnosol	−5.435	−0.151	5.284	4.3777

3.9. Mechanism of corrosion inhibition

By adsorption at the interface between the Cu and solution, the (ROE) compound inhibited corrosion of Cu in 1 M HNO3 using electrochemical tests and mass loss experiments. During the mechanism of action of an (ROE) inhibitor, the inhibitor adsorption at the surface of the metal interface is regarded as the initial stage. There are four ways that organic substances can adsorb on a metal surface, namely:

1. Charged molecules interact electrostatically with charged metals.
2. Molecular electrons interact with metals through their lone pairs.
3. Interaction of π electrons with metal.
4. A combination of the above (Chaouiki et al., 2022). Complete adsorption (a combination of all adsorption types mentioned above) was found for inhibitors adsorbing on the surface of Cu, based on adsorption parameters calculated.

It is possible to form coordinated bonds with the inhibitory molecules by electrons transferring from the adsorbed species to the metal surface. Taking a look at the constitution of the examined compound, it was noted that in all compounds there

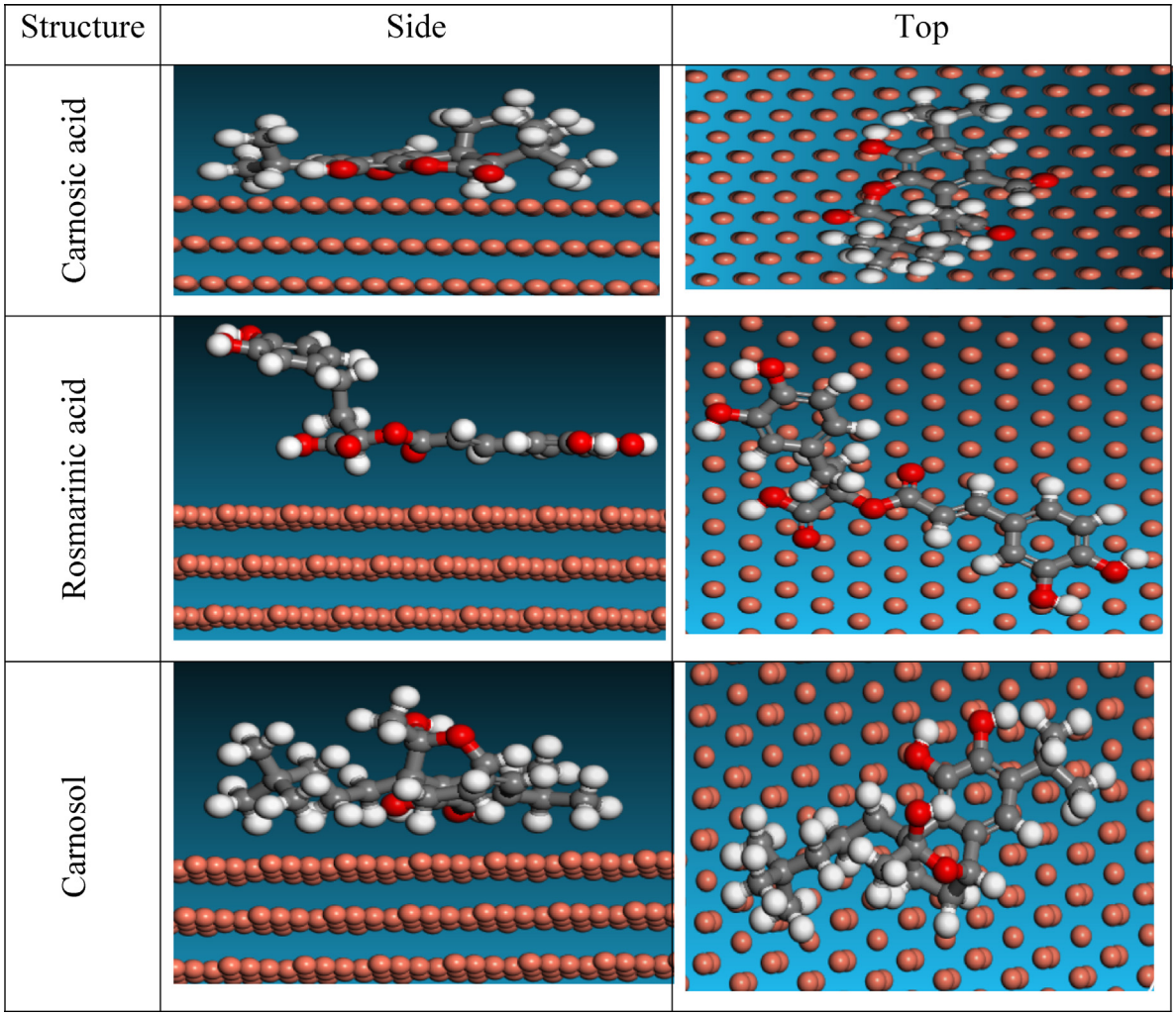

Fig. 9 Top and Side View of adsorption of ROE components on Cu surface.

Table 9 Estimated energies from adsorption of ROE on Cu surface.

Structures	Total energy	Binding energy	Rigid adsorption energy	Deformation energy
Carnosic acid	−64.8866	−87.2233	−91.5315	4.3082
Rosmarinic acid	−177.2225	−104.4682	−105.0472	0.5790
Carnosol	−151.6792	−97.5361	−99.1319	1.5957

are pairs of unshared electrons in oxygen atoms creating a σ-bond with copper. In addition, the double bonds in the substance aid d electrons of metal to be donated back to the π* orbital (Cao et al., 2019; Cao et al., 2020). Inhibitors' efficiency on copper surfaces and effectiveness are all affected by all of this, which depends largely on their type and quantity (Abdel Hameed et al., 2020; Omran and Abdel-Salam, 2020).

4. Conclusions

In experiments, it was proven that (ROE) works as a mixed-type inhibitor to inhibit copper corrosion in 1.0 M HNO_3 solution. This compound exhibited Langmuir adsorption isotherms upon adsorption on copper surfaces, which corresponds to inhibition. The spontaneity of the reaction was inferred due to the presence of the negative value of ΔG^0_{ads}. Using DFT, it was found that the compound has a greater inhibition strength (ROE) because it can transfer electrons from the highest occupied orbital to the lowest unoccupied orbital (LUMO). During corrosion, metal receives electrons from compounds depending on their relative electron donation abilities. A comparison between the results and the measurements was found to be successful.

Declaration of Competing Interest

The authors declare that they have no known competing financial interests or personal relationships that could have appeared to influence the work reported in this paper.

References

Abd El Aziz, S.F., Etaiw, S.E.H., Sobhy, S., 2022. Metal-organic frameworks based on heterocyclic ligands and some transition metals as effective carbon steel corrosion inhibitors in aqueous environment. J. Mol. Liq. 348, 118402.

Abdel Hameed, R.S., Al-Bagawi, A., Shehata, H.A., Shamroukh, A. H., Abdallah, M., 2020. Corrosion inhibition and adsorption properties of some heterocyclic derivatives on C-steel surface in HCl. J. Bio- Tribo-Corrosion 6 (2), 1–11.

Agboola, O., Kupolati, K.W., Fayomi, O.S.I., Ayeni, A.O., Ayodeji, A., Akinmolayemi, J.J., Olagoke, O., Sadiku, R., Oluwasegun, K. M., 2022. A Review on corrosion in concrete structure: inhibiting admixtures and their compatibility in concrete. J. Bio-Tribo-Corrosion 8 (1), 1–22.

Al Jahdaly, B.A., Elsadek, M.F., Ahmed, B.M., Farahat, M.F., Taher, M.M., Khalil, A.M., 2021. Outstanding graphene quantum dots from carbon source for biomedical and corrosion inhibition applications: a review. Sustainability 13 (4), 2127.

Alaoui, K., El Kacimi, Y., Galai, M., Touir, R., Dahmani, K., Harfi, A., Touhami, M.E., 2016. Anti-corrosive properties of polyvinyl-alcohol for carbon steel in hydrochloric acid media: electrochemical and thermodynamic investigation. J. Mater. Environ. Sci 7 (7), 2389–2489.

Alaoui, K., Kacimi, Y. E., Galai, M., Dahmani, K., Harfi, A.E., Touhami, M.E., 2016. Poly (1-phenylethene): as a novel corrosion inhibitor for carbon steel/hydrochloric acid interface.

Bedair, M.A., Abuelela, A.M., Zoghaib, W.M., Mohamed, T.A., 2021. Molecular structure, tautomer's, reactivity and inhibition studies on 6-Methyl-2-thiouracil for mild steel corrosion in aqueous HCl (1.00 M): experimental and theoretical studies. J. Mol. Struct. 1244, 130927.

Belakhdar, A., Ferkous, H., Djellali, S., Sahraoui, R., Lahbib, H., Amor, Y.B., Erto, A., Balsamo, M., Benguerba, Y., 2020. Computational and experimental studies on the efficiency of Rosmarinus officinalis polyphenols as green corrosion inhibitors for XC48 steel in acidic medium. Colloids Surf. A: Physicochem. Eng. Aspects 606, 125458.

Benarioua, M., Mihi, A., Bouzeghaia, N., Naoun, M., 2019. Mild steel corrosion inhibition by Parsley (Petroselium Sativum) extract in acidic media. Egypt. J. Petroleum 28 (2), 155–159.

Boukaoud, A., Chiba, Y., Sebbar, D., 2021. A periodic DFT study of IR spectra of amino acids: An approach toward a better understanding of the NH and OH stretching regions. Vib. Spectrosc. 116, 103280.

Cao, S., Liu, D., Ding, H., Wang, J., Lu, H., Gui, J., 2019. Corrosion inhibition effects of a novel ionic liquid with and without potassium iodide for carbon steel in 0.5 M HCl solution: an experimental study and theoretical calculation. J. Mol. Liq. 275, 729–740.

Cao, S., Liu, D., Ding, H., Lu, H., Gui, J., 2020. Towards understanding corrosion inhibition of sulfonate/carboxylate functionalized ionic liquids: an experimental and theoretical study. J. Colloid Interface Sci. 579, 315–329.

Chaouiki, A., Chafiq, M., Al-Moubaraki, A.H., Bakhouch, M., El Yazidi, M., Ko, Y.G., 2022. Electrochemical behavior and interfacial bonding mechanism of new synthesized carbocyclic inhibitor for exceptional corrosion resistance of steel alloy: DFTB, MD and experimental approaches. Arabian J. Chem. 104323.

Charoen-amornkitt, P., Suzuki, T., Tsushima, S., 2020. Effects of voltage-dependence of the constant phase element and ohmic parameters in the modeling and simulation of cyclic voltammograms. J. Electrochem. Soc. 167, (16) 166506.

Chen, S., Chen, S., Zhu, B., Huang, C., Li, W., 2020. Magnolia grandiflora leaves extract as a novel environmentally friendly inhibitor for Q235 steel corrosion in 1 M HCl: combining experimental and theoretical researches. J. Mol. Liq. 311, 113312.

Chen, S., Zhu, B., Liang, X., 2020. Corrosion inhibition performance of coconut leaf extract as a green corrosion inhibitor for X65 steel in hydrochloric acid solution. Int. J. Electrochem. Sci 15 (1), 1.

Chkirate, K., Azgaou, K., Elmsellem, H., El Ibrahimi, B., Sebbar, N. K., Benmessaoud, M., El Hajjaji, S., Essassi, E.M., 2021. Corrosion inhibition potential of 2-[(5-methylpyrazol-3-yl) methyl] benzimidazole against carbon steel corrosion in 1 M HCl solution: combining experimental and theoretical studies. J. Mol. Liq. 321, 114750.

Choudhary, V., Bhatt, A., Dash, D., Sharma, N., 2019. DFT calculations on molecular structures, HOMO–LUMO study, reactivity descriptors and spectral analyses of newly synthesized diorganotin (IV) 2-chloridophenylacetohydroxamate complexes. J. Computational Chem. 40 (27), 2354–2363.

Dhouibi, I., Masmoudi, F., Bouaziz, M., Masmoudi, M., 2021. A study of the anti-corrosive effects of essential oils of rosemary and myrtle for copper corrosion in chloride media. Arabian J. Chem. 14, (2) 102961.

El Faydy, M., Galai, M., Touir, R., El Assyry, A., Ebn Touhami, M., Benali, B., 2016. Experimental and theoretical studies for steel XC38 corrosion inhibition in 1 M HCl by N-(8-hydroxyquinolin-5-yl)-methyl)-N-phenylacetamide. J. Mater. Environ. Sci. 7 (4), 1406–1416.

Erigoni, A., 2021. Organic-inorganic hybrid catalysts for chemical processes of industrial interest. Universitat Politècnica de València.

Errahmany, N., Rbaa, M., Abousalem, A.S., Tazouti, A., Galai, M., Touhami, M.E., Lakhrissi, B., Touir, R., 2020. Experimental, DFT calculations and MC simulations concept of novel quinazolinone derivatives as corrosion inhibitor for mild steel in 1.0 M HCl medium. J. Mol. Liq. 312.

Esmeeta, A., Adhikary, S., Dharshnaa, V., Swarnamughi, P., Maqsummiya, Z.U., Banerjee, A., Pathak, S., Duttaroy, A.K., 2022. Plant-derived bioactive compounds in colon cancer treatment: An updated review. Biomed. Pharmacother. 153, 113384.

Fergachi, O., Benhiba, F., Rbaa, M., Ouakki, M., Galai, M., Touir, R., Lakhrissi, B., Oudda, H., Touhami, M.E., 2019. Corrosion inhibition of ordinary steel in 5.0 M HCl medium by benzimidazole derivatives: electrochemical, UV–visible spectrometry, and DFT calculations. J. Bio-Tribo-Corrosion 5 (1), 1–13.

Fouda, A., Badr, S., Ahmed, A., El-Hossiany, A., 2021. Chemical and electrochemical corrosion of a copper alloy in aqueous solutions by using morus alba extract as an eco-friendly inhibitor. Int. J. Corrosion Scale Inhibition 10 (3), 1011–1029.

Galai, M., Ouassir, J., Ebn Touhami, M., Nassali, H., Benqlilou, H., Belhaj, T., Berrami, K., Mansouri, I., Oauki, B., 2017. α-Brass and (α+ β) brass degradation processes in Azrou soil medium used in plumbing devices. J. Bio- Tribo-Corrosion 3 (3), 1–15.

Galai, M., Rbaa, M., Ouakki, M., Abousalem, A.S., Ech-Chihbi, E., Dahmani, K., Dkhireche, N., Lakhrissi, B., EbnTouhami, M., 2020. Chemically functionalized of 8-hydroxyquinoline derivatives as efficient corrosion inhibition for steel in 1.0 M HCl solution: experimental and theoretical studies. Surf. Interfaces 21, 100695.

Hadisaputra, S., Purwoko, A.A., Savalas, L.R.T., Prasetyo, N., Yuanita, E., Hamdiani, S., 2020. Quantum chemical and Monte Carlo simulation studies on inhibition performance of caffeine and its derivatives against corrosion of copper. Coatings 10 (11), 1086.

Hamadi, L., Mansouri, S., Oulmi, K., Kareche, A., 2018. The use of amino acids as corrosion inhibitors for metals: a review. Egyptian J. Petroleum 27 (4), 1157–1165.

Hoffman, B.C., 2019. copper alloying practices at the indus tradition site of Harappa. Ancient Sindh Annu. Res. J. 15 (15), 7.

Huang, L., Chen, W.-Q., Wang, S.-S., Zhao, Q., Li, H.-J., Wu, Y.-C., 2022. Starch, cellulose and plant extracts as green inhibitors of metal corrosion: a review. Environ. Chem. Lett., 1–30

Hussain, C.M., 2020. The handbook of environmental remediation: classic and modern techniques. Roy. Soc. Chem.

Jafari, H., Rezaeivala, M., Mokhtarian, N., Berisha, A., Ameri, E., 2022. Corrosion inhibition of carbon steel in 0.5 M H2SO4 by new reduced Schiff base ligand. J. Bio- Tribo-Corrosion 8 (3), 1–13.
Jiang, J., Zhang, S., Longhurst, P., Yang, W., Zheng, S., 2021. Molecular structure characterization of bituminous coal in Northern China via XRD, Raman and FTIR spectroscopy. Spectrochimica Acta Part A: Mol. Biomol. Spectrosc. 255, 119724.
Kadhim, A., Al-Amiery, A., Alazawi, R., Al-Ghezi, M., Abass, R., 2021. Corrosion inhibitors. A review. Int. J. Corrosion Scale Inhibition 10 (1), 54–67.
Kadiri, L., Galai, M., Ouakki, M., Essaadaoui, Y., Ouass, A., Cherkaoui, M., Rifi, E.-H., Lebkiri, A., 2018. Coriandrum Sativum. L seeds extract as a novel green corrosion inhibitor for mild steel in 1.0 M hydrochloric and 0.5 M sulfuric solutions. Anal. Bioanal. Electrochem. 10, 249–268.
Karolina, D., Maja, M.-S., Magdalena, D.-S., Grażyna, Ż., 2022. Identification of treated Baltic amber by FTIR and FT-Raman–a feasibility study. Spectrochimica Acta Part A: Mol. Biomol. Spectrosc., 121404
Kompelly, A., Kompelly, S., Vasudha, B., Narender, B., 2019. Rosmarinus officinalis L.: an update review of its phytochemistry and biological activity. J. Drug Delivery Therapeutics 9 (1), 323–330.
Kumari, V., Singh, P.P., Kaushal, S., 2022. Synthesis and applications of metal-organic frameworks and graphene-based composites: a review. Polyhedron 115645.
Laschuk, N.O., Easton, E.B., Zenkina, O.V., 2021. Reducing the resistance for the use of electrochemical impedance spectroscopy analysis in materials chemistry. RSC Adv. 11 (45), 27925–27936.
Loto, R.T., 2020. Evaluation of the corrosion inhibition effect of the combined admixture of rosemary and cinnamon cassia oil on mild steel in weak acid electrolyte. Sustainable Chem. Pharm. 17, 100298.
Loto, R.T., Loto, C.A., Fajobi, M., Olanrewaju, G., 2022. Comparative assessment and statistical data of admixed rosemary and castor oil on the corrosion inhibition of high carbon and P4 low carbon mold steels. Mater. Today: Proc. 49, 1926–1931.
Marques, A.C., Mocanu, A., Tomić, N.Z., Balos, S., Stammen, E., Lundevall, A., Abrahami, S.T., Günther, R., de Kok, J.M., Teixeira de Freitas, S., 2020. Review on adhesives and surface treatments for structural applications: Recent developments on sustainability and implementation for metal and composite substrates. Materials 13 (24), 5590.
Mintz, K.J., Bartoli, M., Rovere, M., Zhou, Y., Hettiarachchi, S.D., Paudyal, S., Chen, J., Domena, J.B., Liyanage, P.Y., Sampson, R., 2021. A deep investigation into the structure of carbon dots. Carbon 173, 433–447.
Miraj, S., Kiani, S., 2016. A review study of therapeutic effects of Salvia officinalis L. Der Pharmacia Lettre 8 (6).
Niamien, P., Essy, F., Trokourey, A., Yapi, A., Aka, H., Diabate, D., 2012. Correlation between the molecular structure and the inhibiting effect of some benzimidazole derivatives. Mater. Chem. Phys. 136 (1), 59–65.
Obi-Egbedi, N., Obot, I., El-Khaiary, M.I., 2011. Quantum chemical investigation and statistical analysis of the relationship between corrosion inhibition efficiency and molecular structure of xanthene and its derivatives on mild steel in sulphuric acid. J. Mol. Struct. 1002 (1–3), 86–96.
Odunlami, O., Loto, R., Fajobi, M., Olomukoro, O., Akande, I., Oke, M., Oladimeji, T., 2021. Data on the corrosion Inhibition Property of Rosemary on High Carbon Steel in dilute sulphuric acid, citric acid and sodium chloride solution. Chemical Data Collections 32, 100660.
Omran, B.A., Abdel-Salam, M.O., 2020. A New Era for Microbial Corrosion Mitigation Using Nanotechnology. Springer.
Onyeachu, I.B., Njoku, D.I., Kaya, S., El Ibrahimi, B., Nnadozie, C. F., 2022. Sour corrosion of C1018 carbon steel and its inhibition by 1–benzylimidazole: electrochemical, SEM, FTIR and computational assessment. J. Adhesion Sci. Technol. 36 (7), 774–794.
Pal, A., Das, C., 2022. New eco-friendly anti-corrosion inhibitor of purple rice bran extract for boiler quality steel: experimental and theoretical investigations. J. Mol. Struct. 1251, 131988.
Palanisamy, G., 2019. Corrosion inhibitors. Corrosion inhibitors, 24.
Rodríguez-Valdez, L.M., Martínez-Villafañe, A., Glossman-Mitnik, D., 2005. Computational simulation of the molecular structure and properties of heterocyclic organic compounds with possible corrosion inhibition properties. J. Mol. Struct.: THEOCHEM 713 (1–3), 65–70.
Saleh, T.A., Haruna, K., Nur, M.M., Alharbi, B., 2022. Synthesis of Amine Grafted Poly (Acrylic-Maleic) as an efficient inhibitor against stainless steel corrosion in a highly saline medium. Prog. Organic Coatings 170, 106974.
Sayed, A.R., El-Lateef, H.M.A., 2020. Thiocarbohydrazones based on adamantane and ferrocene as efficient corrosion Inhibitors for hydrochloric acid pickling of C-steel. Coatings 10 (11), 1068.
Scott, D.A., Schwab, R., 2019. The Metallurgy of Pre-industrial Metals and Alloys. In: Metallography in Archaeology and Art. Springer, pp. 133–206.
Shahmoradi, A., Ranjbarghanei, M., Javidparvar, A., Guo, L., Berdimurodov, E., Ramezanzadeh, B., 2021. Theoretical and surface/electrochemical investigations of walnut fruit green husk extract as effective inhibitor for mild-steel corrosion in 1M HCl electrolyte. J. Mol. Liq. 338, 116550.
Singh, A., Ansari, K., Lin, Y., Quraishi, M., Lgaz, H., Chung, I.-M., 2019. Corrosion inhibition performance of imidazolidine derivatives for J55 pipeline steel in acidic oilfield formation water: Electrochemical, surface and theoretical studies. J. Taiwan Institute Chem. Engineers 95, 341–356.
Xiao, J., Long, X., Qu, W., Li, L., Jiang, H., Zhong, Z., 2022. Influence of sulfuric acid corrosion on concrete stress–strain relationship under uniaxial compression. Measurement 187, 110318.
Yan, T., Zhang, S., Feng, L., Qiang, Y., Lu, L., Fu, D., Wen, Y., Chen, J., Li, W., Tan, B., 2020. Investigation of imidazole derivatives as corrosion inhibitors of copper in sulfuric acid: combination of experimental and theoretical researches. J. Taiwan Institute Chem. Engineers 106, 118–129.
Yang, F., Kang, H., Chen, Z., Guo, E., Zeng, Y., Wang, W., Wang, T., 2019. Electrochemical corrosion mechanisms of nickel-aluminium bronze with different nickel contents using the rotating disc electrode. Corrosion Sci. 157, 438–449.
Zhang, Y., Tan, B., Guo, L., Zhu, M., 2022. Controllable fabrication of carbon dots based corrosion inhibitors with fluorescence properties. In: Eco-Friendly Corrosion Inhibitors, Elsevier, pp. 505-526.
Zhang, W., Li, H.-J., Wang, M., Wang, L.-J., Zhang, A.-H., Wu, Y.-C., 2019. Highly effective inhibition of mild steel corrosion in HCl solution by using pyrido [1, 2-a] benzimidazoles. New J. Chem. 43 (1), 413–426.
Zhang, X., Li, W., Yu, G., Zuo, X., Luo, W., Zhang, J., Tan, B., Fu, A., Zhang, S., 2020. Evaluation of Idesia polycarpa Maxim fruits extract as a natural green corrosion inhibitor for copper in 0.5 M sulfuric acid solution. J. Mol. Liq. 318, 114080.
Zhang, D., Zhang, H., Zhao, S., Li, Z., Hou, S., 2019. Electrochemical impedance spectroscopy evaluation of corrosion protection of X65 carbon steel by halloysite nanotube-filled epoxy composite coatings in 3.5% NaCl solution. Int. J. Electrochem. Sci 14, 4659–4667.
Zhang, Y., Zhang, S., Tan, B., Guo, L., Li, H., 2021. Solvothermal synthesis of functionalized carbon dots from amino acid as an eco-friendly corrosion inhibitor for copper in sulfuric acid solution. J. Colloid Interface Sci. 604, 1–14.
Zuñiga-Diaz, K., Arrieta-Gonzalez, C., Porcayo-Calderon, J., Gonzalez-Rodriguez, J., Casales-Diaz, M., Martinez-Gomez, L., 2020. Electrochemical behavior of austenitic stainless steels exposed to acetic acid solution. Int. J. Electrochem. Sci 15, 1242–1263.